ACS OMEGA

http://pubs.acs.org/journal/acsodf

Article

Graphene Oxide-Induced Interfacial Transcrystallization of Single-Fiber Milkweed/Polycaprolactone/Polyvinylchloride Composites

Phuong Nguyen-Tri,* Pascal Carrière, Adam Duong, and Sonil Nanda

Cite This: *ACS Omega* 2020, 5, 22430−22439

Read Online

ACCESS | Metrics & More | Article Recommendations

ABSTRACT: Understanding the interfacial crystallization is crucial for semi-crystalline polymer/natural fiber composites because it links to the final properties. This work reports, for the first time, the interfacial crystallization of a miscible blend between polycaprolactone (PCL) and polyvinylchloride (PVC) with milkweed fibers. We have first described the morphology of the fibers and the chemical composition of waxes covered on its surface. Our findings show that the transcrystallization (TC) layer of PCL/PVC could appear at the interface by simply coating with a layer of graphene oxide (GO) on the milkweed fiber. In our study, atomic force microscopy−infrared spectroscopy analysis shows that the crystallinity of the blends is higher at the vicinity of the interface compared to that in the bulk. The kinetic of the interfacial crystallization in terms of spherulite morphology and crystal growth rates at the nanoscale is examined. X-ray photoelectron spectroscopy and high-resolution transmission electron microscopy were used to analyze the prepared GO and evaluate its relationship with the interfacial crystallization behavior of the blends.

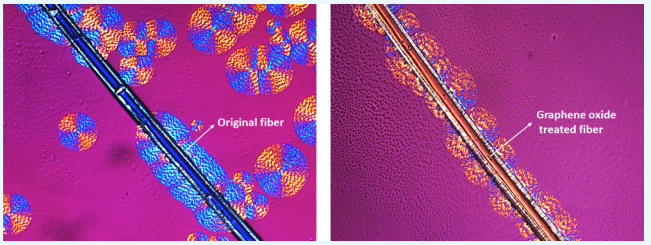

1. INTRODUCTION

The investigation of the crystallization phenomena is crucial to better understand the morphology and final properties of a polymeric blend. In recent decades, the crystallization of thermoplastic polymeric blends has been extensively studied[1−3] and it still constitutes a fascinating and fruitful field of research.[2−6] Recent progress in the nanoscale characterization methods, such as atomic force microscopy (AFM)[7] and small-angle X-ray scattering, have helped to highlight various scientific questions related to molecular architectures, lamella assembly, distribution, and phase separation in a polymeric spherulite structure.[8] However, a deep understanding of these phenomena becomes more complicated for miscible blends in which the phase separation cannot be distinguished using morphological analysis tools. Moreover, the miscible crystalizable/amorphous blends can display various morphologies and crystallization mechanisms depending upon blend ratios and crystallization processes. The amorphous component can be rejected inside or outside of the spherulite growth as described in our previous publications.[9−11] Atomic force microscopy infrared-spectroscopy (AFM-IR) has recently been reported as a useful tool that can provide both nanoscale morphology and chemical information of the polymeric materials[12−18] including biopolymers.[19]

Polycaprolactone (PCL) is widely used in various biomedical applications, including artificial skin,[20] resorbable prostheses,[10,21] fast drug delivery,[22] tissue engineering,[23] and pharmaceutical formulations,[22] because of its biocompatibility, biodegradability, and nontoxicity (i.e., FDA-approved).[24] The addition of polyvinyl chloride (PVC) into the PCL matrix is reported to enhance its flexibility, mechanical strength, and stability under high-energy irradiation, making it more suitable for flexible medical products.[25] They form miscible blends in whole blend contents[26,27] because of the dipole−dipole interactions between carbonyl and C−Cl groups.[4] However, the presence of the PVC may disturb the crystallization of the PCL in terms of the spherulitic growth rate and morphology. It has been reported that regular or inverted S- or C-shaped crystals are observed in the miscible PCL/PVC blends instead of the truncated lozenge-shape morphology as is usually observed in the case of pure poly (ε-caprolactone) (PCL), and the crystal curvature is controllable by the nature of the second polymer and blend composition.[28] The growth rate of PCL crystals was strongly depressed with the addition of PVC in the blend because of a significant difference in terms of polarity between these two polymers.[26,29] During the crystallization of PCL/PVC blends, the segregation of the polymer can occur, which leads to a concentration gradient of two components. The PCL-rich areas are found close to the air-polymer interface while the PVC-rich areas are found in deeper areas.[26]

Received: June 17, 2020
Accepted: August 11, 2020
Published: August 27, 2020

https://dx.doi.org/10.1021/acsomega.0c02913
ACS Omega 2020, 5, 22430−22439

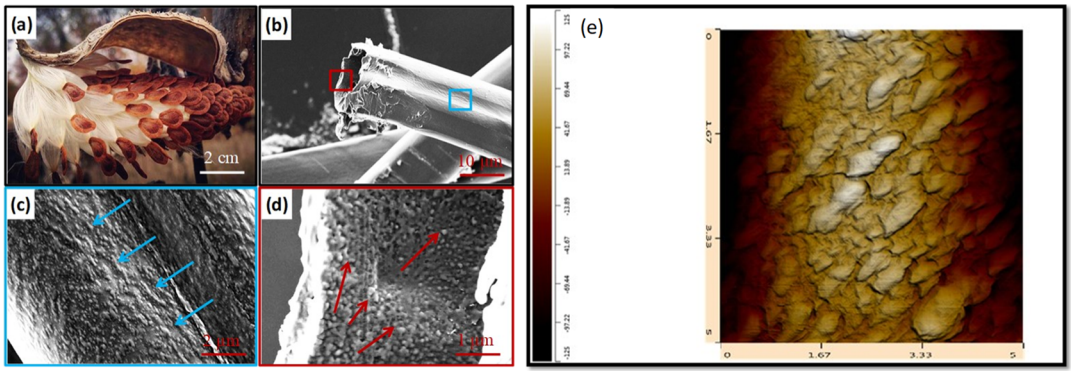

Figure 1. Morphology of milkweed fibers: (a) naturally occurring in the wild; (b) SEM image of a fiber surface at low magnification showing its hollow structure; (c) SEM image of the outer surface; (d) inter surface of the fiber showing a rough surface which is naturally covered by waxes; and (e) high-resolution AFM images of the original milkweed fiber surface showing the morphology of the waxes on the fiber surface. From this image, the three-dimensional rugosity index is calculated using AFM-IR software. The arrows in (c,d) show the presence of wax inside and outside the fiber surface.

The examination of the distribution and segregation mechanism of the components in the PCL/PVC blends at the sub-micrometer scale remains an open question, despite the progress made in spectroscopic and morphological analyses for polymeric blends. This issue becomes more complicated when a long fiber is added in the blends, especially at the interface because of chemical interactions. The crystals, appearing at the interface, are often different from those in the bulk. They form a highly ordered structure, grown perpendicularly to the fiber surface, which is called the transcrystallization layer.[30−33] Some recent publications have mostly concentrated on the formation mechanisms and morphology of the transcrystallization layers.[31−34] However, the detailed analysis of transcrystallization in terms of growth rate and chemical composition of the blends at the polymer/fiber interface, especially at the nanoscale level is lacking. The effect of the PVC on the crystallization of the PCL at the interface and in the bulk is crucial because it will directly relate to the properties and the durability of the service of final products. Moreover, the transcrystallization of PCL/PVC blends on the surface of the natural fiber is not yet reported in the literature.

The exploitation of novel, abundant, and renewable biomaterials with special properties from natural products acquires great attention for both manufacturers and researchers beause of their lower carbon footprints. Milkweed fibers (*Asclepiad* fiber) are considered as perennial plants with umbel-like flowers, which are abundant in North America. Milkweed fibers have recently been used for many domestic and industrial purposes such as isolating fabrics, water/oil separation membranes, ecological, and nonfur/nonleather winter garments.[35,36] These fibers are special because they have low densities (4−5 times lighter than jute fiber), represented by microscale hollow tubes (Figure 1b) and exhibit a rough surface naturally covered by superhydrophobic waxes (Figure 1c,d). These properties make materials suitable for low-density composite materials for various applications, especially in the automobile industry. However, there is limited information in the literature about the structure and morphology of composites reinforced by these fibers, especially at the nanoscale level.

Recently, we have successfully used AFM-IR to shed light on some scientific questions related to: (i) the aging mechanism at the surface of organic coatings;[37] (ii) the complementary understanding of the aging mechanism of a polyester fiber;[38] (iii) the grafting of the polyvinyl pyridine-like polymeric film on a titanium nitride wafer;[39] and (iv) the crystallization behavior of immiscible[10] and miscible blends.[11] In this article, AFM-IR in combination with polarized optical microscopy (POM) are mainly used to investigate the transcrystallization phenomena of a PCL/PVC blend with the presence of a single milkweed fiber in terms of the crystal growth mechanism, spherulite morphology, and polymer diffusion. The findings from this study attempts to fill the gaps in the literature. Graphene oxide (GO) was also synthesized and characterized by X-ray photoelectron spectroscopy (XPS) and high-resolution transmission electron microscopy (HR-TEM). They are then coated on the fiber surface to promote the transcrystallization at the fiber interface.

2. RESULTS AND DISCUSSIONS

2.1. Fiber Characterization. Milkweed fibers are considered as a perennial plant with umbel-like flowers, which are abundant in Quebec and most of North America (Figure 1a). However, the inside and outside morphologies of these fibers, especially at the nanoscale level, are not yet reported in the literature. SEM observations of these fibers show that they are hollowed (Figure 1b) and the average dimension of the fiber is found to be 18 ± 7 μm with a cell wall thickness of 900 ± 120 nm including the wax layer thickness (Figure 1b). Higher magnification of SEM images allows observing the outside (Figure 1c) and inside surfaces (Figure 1d). The original fiber shows a rough surface naturally covered by waxes on both faces including inside and outside of the fiber. High-resolution three-dimensional AFM image on the outer fiber surface (Figure 1e) shows that the wax crystals exhibit a dimension of 80−150 nm in height and 400−700 nm in width.

From these images, the rugosity index is calculated to be 1.25 ± 0.3. The removal of these waxes by chloroform leads to the development of a smooth fiber surface, as determined by AFM profile measurements, thus allowing direct contact between the polymer matrix and the fiber surface. The chemical analysis of the waxes extracted by GC−MS (data not shown) indicates that they contain mainly aromatic phenols (C_{16-20}), which are different from aliphatic alcohols (C_{16}−C_{20}), mainly found in another superhydrophobic material such as lotus leaves.[41,42] The detailed composition of the milkweed can be found in some recent publications.[43,44]

https://dx.doi.org/10.1021/acsomega.0c02913
ACS Omega 2020, 5, 22430−22439

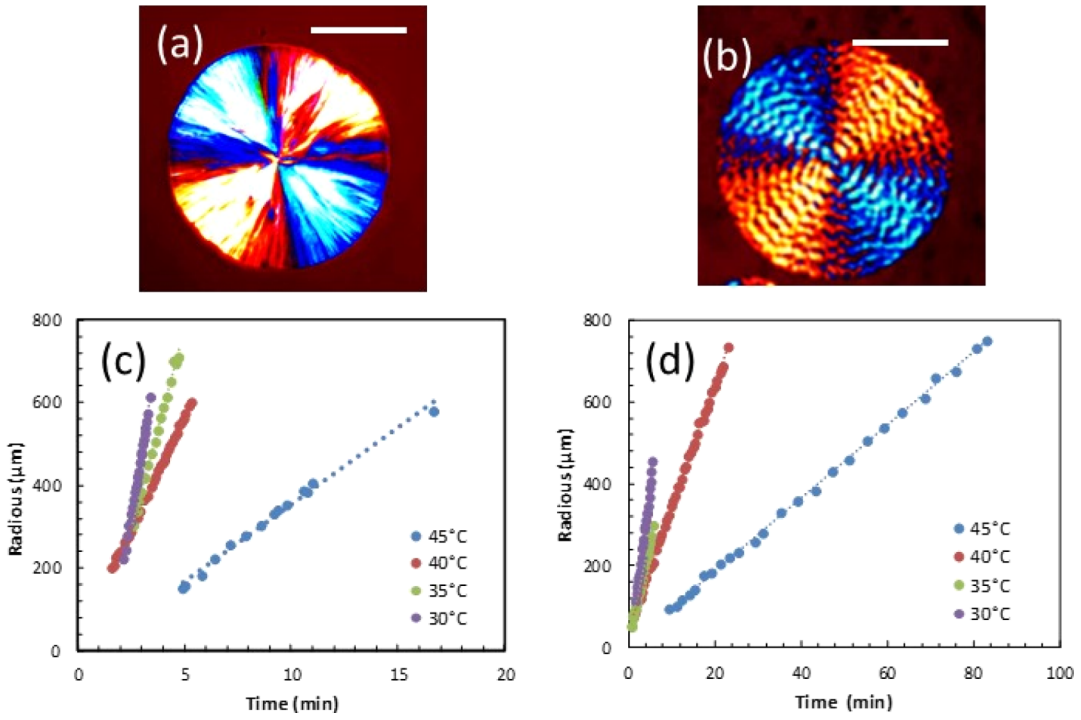

Figure 2. POM images showing the spherulite morphology of (a) neat PCL and (b) PCL/PVC (80/20), isothermally crystallized at 45 °C, for 3 min and 22 min, respectively; (c) spherulite growth rate of neat PCL, and (d) growth rate of the PCL/PVC (80/20) blend at different temperatures. Scale bars in (a,b) are of 100 μm.

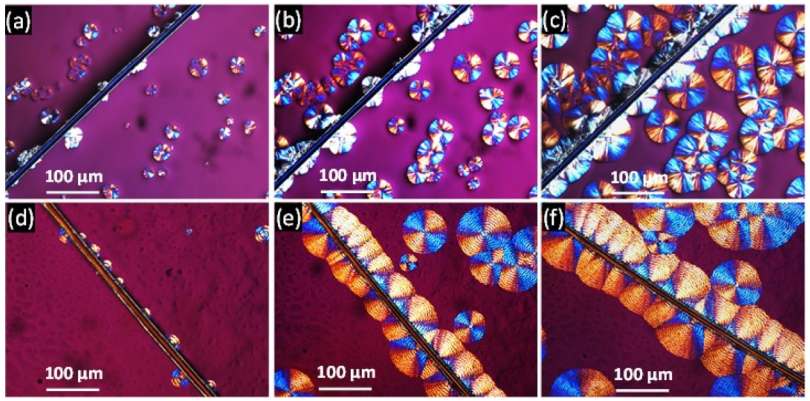

Figure 3. POM images showing spherulite evolution as a function of isothermal crystallization times (35 °C) for: neat PCL: (a) 1 min, (b) 2 min, and (c) 3 min and for the PCL/PVC (80/20) blend: (d) 1 min, (e) 2 min, and (f) 3 min.

2.2. Crystallization Behavior of Neat PCL/PVC Blends.

The crystallization of neat PCL and PCL/PVC (80/20) blends was investigated in terms of spherulitic morphology and growth rate at different crystallization temperatures and times. Figure 2 shows the POM images of neat PCL (Figure 2a) and PCL/PVC (80/20) blends (Figure 2b). In the case of neat PCL, the spherulite exhibits a well-defined spherical shape with a Maltese cross. The alternation of dark and light colors in the spherulitic structure, observed under polarized microscopy (POM), is due to the birefringence of PCL with anisotropy of crystalline lamellae.[45] For the PCL/PVC (80/20) blend, the spherulite morphology is different from that observed in neat PCL. Although the Maltese cross is observed, the spherulites are banded and smaller compared to those observed for neat PCL. Under certain conditions, the spherulites of certain semi-crystalline polymers exhibit concentric bands or rings (banded spherulites).[46] Several reasons give rise to these banded structures. First, they could be because of a twist of the lamellar chains around their growth axis. This lamellar twist leads to a modification of the refractive index according to the orientation of the crystalline planes.[47] Second, this could be because of a rhythmic variation in the thickness of the spherulites during growth, causing bands of regular extinctions to appear.[46] This phenomenon could be explained by competition between the diffusion and the consumption of polymer chains during the crystallization, as described in our previous publications.[10,11]

The evolution of the spherulite radius as a function of time for neat PCL and PCL/PVC (80/20) blends was studied by measuring the spherulite radius with crystallization time. For neat PCL (Figure 2c), the spherulite radius linearly increases with crystallization time. Similarly, at a given blend composition and crystallization temperature, the radius of spherulites of the PCL/PVC (80/20) blend evolves linearly

https://dx.doi.org/10.1021/acsomega.0c02913
ACS Omega 2020, 5, 22430−22439

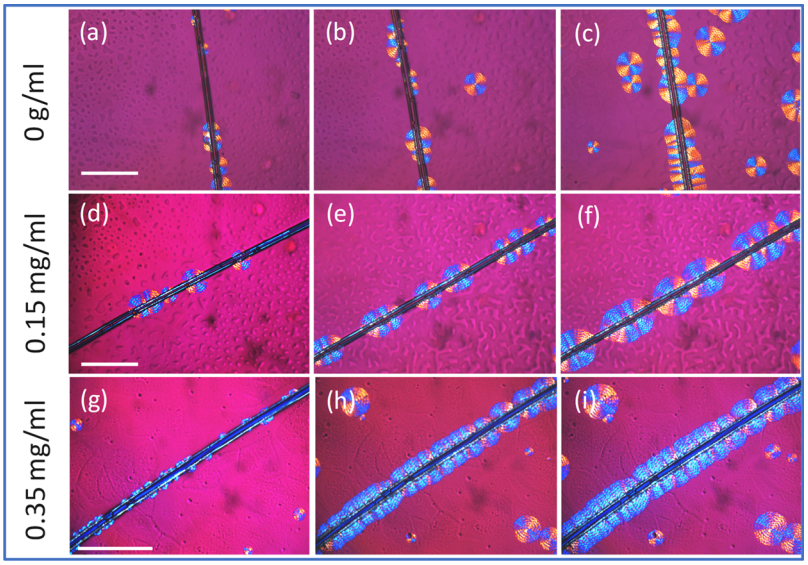

Figure 4. POM images showing the development of the transition layer at the composite interface with different treatment methods as a function of the isothermal crystallization times: (i) first row: fiber treated with only distilled water: (a) 1 min; (b) 2 min; and (c) 3 min; (ii) second row: fiber treated with a solution of 0.15 mg/mL of GO in distilled water: (d) 1 min; (e) 2 min; and (f) 3 min, (iii) third row: fiber treated with a solution of 0.35 mg/mL of GO in distilled water: (g) 1 min; (h) 2 min; and (i) 3 min. Scale bars are of 150 μm. The chemical composition of PCL/PVC = 80/20. Treatment time of the fiber with the GO solution is of 5 min. Isothermal crystallization at 45 °C.

with crystalization time (Figure 2d). Thanks to these linear relations, the growth rates of spherulites of neat PCL and PCL/PVC (80/20) blends were calculated by extrapolating the linear curves. For the hereby studied crystallization temperatures ranging from 30 to 45 °C, a decrease in the crystallization temperature leads to an increase of the spherulitic growth rate for both neat PCL and PCL/PVC blends.

The growth rate was significantly dependent upon the increasing crystallization temperature. This is because the PCL has a relatively low melting temperature (about 60 °C) and the crystallization of PCL was not thermodynamically favored at high temperatures. The addition of PVC significantly slows down the growth rate of the PCL spherulite. Isothermal crystallization of the neat PCL at 35 °C exhibits a spherulitic growth rate of 202 μm/min, while this value was decreased to 46 μm/min for the PCL/PVC (80/20) blend at the same crystallization conditions.

2.3. Interfacial Crystallization of Composites. Figure 3 shows an example of the evolution of the spherulitic growth rate as a function of crystallization time for neat PCL (Figure 3a–c) and PCL/PVC (80/20) blends (Figure 3d–f) in the presence of a single milkweed fiber. For the neat PCL matrix, the presence of the fiber has no significant effect on the appearance of the spherulite morphology. Initially, some germinations/crystals nonhomogeneously distributed along with the fiber were observed (Figure 3a). These crystals were then developed to form a semicircular spherulitic layer whose thickness increased with the crystallization time (Figure 3b,c). Because of the lack of abondant germinations on the fiber surface, the spherulites in this interface have a similar morphology to those observed in the bulk.

For the PCL/PVC (80/20) blend, the formation of various germinations was initially observed on the fiber surface (Figure 3d). However, these germinations did not homogenously appear on the whole fiber surface. Moreover, they were not symmetrically developed on both sides of the fiber. They grow slowly in a direction perpendicular to the axis of the fiber to form the transcrystallization layers (Figure 3e,f). Compared to neat PCL, the addition of amorphous PVC shows a notable effect on the crystallization of the PCL. Banded spherulites, which are observed for the PCL/PVC blend, are different from those previously observed for neat PCL. Under special crystallization conditions, several spherulites of semi-crystallin polymers such as polyethylene (PE), poly lactic acid (PLA), polycaprolactone (PC), and polyethylene terephthalate (PET) can exhibit various morphologies, the most common are banded or concentric ring ones.[48] There are several reasons that give birth to these rings. First, they could be because of a twisting of the lamellar chains around their axis of growth. This torsion leads to a modification of the refractive index following the orientation of the crystalline planes.[49] Second, it would be because of a rhythmic variation in the thickness of the spherulites during growth, showing regular extinctions bands[48,50] due to competition between broadcasting and channel consumption during crystallization.[51] In this case, the addition may perturb the crystallization of PCL and lead to the twisting of the lamellar chains of PCL. The latter is favored to the banded spherulites.

The thickness of the transcrystallization layer was measured as a function of time by analyzing POM images to evaluate the effect of the fiber on the growth rate of spherulites at the interface. The obtained results (data not shown) indicated that for a given blend composition, the presence of the fiber did not significantly change the crystallization growth rate of spherulite developed at the fiber interface or in the bulk. In other words, the crystallization rate was similar in the entire sample. The influence of crystallization temperature on the transcrystallization layer was also examined during the crystallization and obtained results are similar to those presented in Figure 2, meaning that the increase of the isothermal crystallization temperature leads to a significant reduction in the thickness of transcrystallization layers. This effect is particularly true at higher crystallization temperatures (45 °C). At 35 °C, the

https://dx.doi.org/10.1021/acsomega.0c02913
ACS Omega 2020, 5, 22430−22439

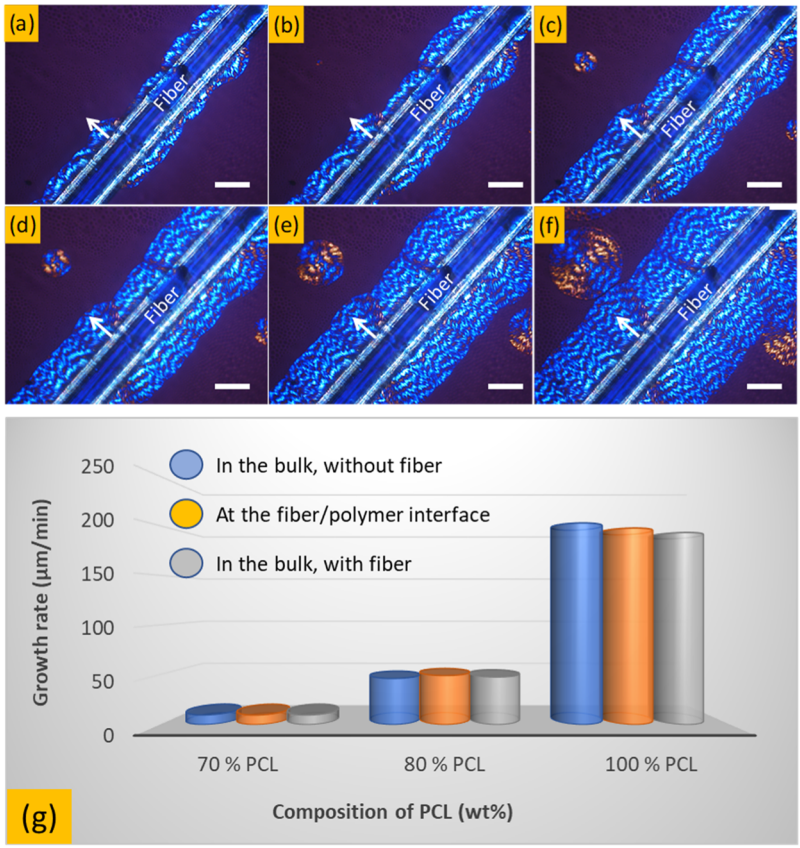

Figure 5. POM images showing the evolution of the transcrystallization layer at the polymer/fiber interface of PCL/PVC (80/20) blend, as a function of crystallization times: (a) 15 s; (b) 30 s; (c) 60 s; (d) 90 s; (e) 120 s and (f) 180 s and (g) growth rates of spherulites at different PCL contents and locations. Scale bars in (a−f) are 20 μm. The neat PCL and PCL/PVC blends were isothermally crystallized at 35 °C.

thickness of the transcrystallization layer of PCL/PVC was measured to be about 400 μm while it has reduced to 120 μm when the crystallization temperature increased to 45 °C under the same crystallization conditions. It is worth mentioning that the development of transcrystallization layers is not continuous and that the measurement of transcrystallization layer should be stopped when a spherulitic boundary between transcrystallization and spherulites in the bulk was achieved.

It has been previously seen that the transcrystallization layer is not always symmetrical with respect to the fiber despite the high density of crystal germs on the fiber surface. In fact, the milkweed fibers are of natural origin, and hence, they do not have a homogeneous distribution of germination to create a transcrystallization layer (Figure 1c). The transcrystallization layer was only induced by a large number of germinations present on the surface of natural fibers, which forces PCL crystals to develop in a single direction, perpendicular to the axis of the fiber.

2.4. Effect of Fiber Treatment on Crystallization Behavior. To promote the formation of the transcrystallization layer on the fiber surface, graphene oxide (GO) was used as a nucleating agent to enhance the transcrystallization on the fiber surface. Graphene oxide (GO) was first synthesized and then coated on to the fiber by dip-coating technique. The fibers' surface was dip-coated with a GO solution in distilled water at different concentrations to control the GO layer formation on the fiber surface.

The GO layer can promote the polymer crystalization by creating homogeneous nucleation sites and the chemical bonding such as hydrogen bonds and dipole−dipole interactions between the functional groups (hydroxyl and carbonyl) on the graphene oxide and the polymers.[32] Figure 4 shows the POM images of the PCL/PVC (80/20) composite near the fiber surface treated with different GO concentrations: 1.5 mg/mL (Figure 4d−f) and 0.35 mg/mL (Figure 4g−i). A fiber treated by only distilled water (0 mg/mL GO concentration) was also added as a control sample (Figure 4a−c).

In the first case, the presence of the fiber has an effect on the spherulite development at the interface; some nucleating sites appeared at the fiber surface to form semicircular spherulites (Figure 4a−c). However, they are not homogeneous as some spherulites are also observed in the bulk. It is interesting to observe that the addition of graphene oxide leads to an increase of the germination sites (Figure 4d−f) and a higher density of spherulites at the interface was observed. The morphology of these spherulites was very similar to that in the bulk, meaning that the lamellar was freely developed in the three-dimensional direction. Further addition of GO (0.35 mg/mL) leads to the formation of a transcrystallization layer in which the spherulites were forced to develop perpendicularly with the fiber surface under confined conditions (Figure 4g−i).

The transcrystallization phenomena are already observed in various semicrystalline polymers, such as polypropylene (PP),[52,53] polyethylene terephthalate (PET),[54] polylactide acid (PLA),[31] and poly(butylene succinate) (PBS).[55] It was probably first observed and described by Jenckel et al.[56,57] in 1952 from which the transcrystallization was induced by a large

https://dx.doi.org/10.1021/acsomega.0c02913
ACS Omega 2020, 5, 22430−22439

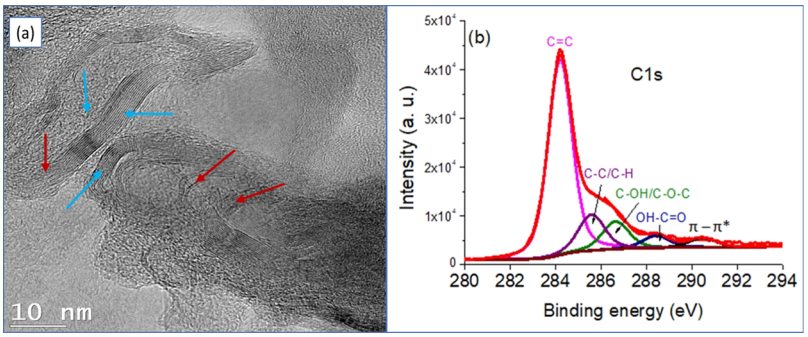

Figure 6. (a) HR-TEM of the prepared GO and (b) C 1s-XPS survey scan of GO layers showing the convolution of oxygen-attached carbon functional groups.

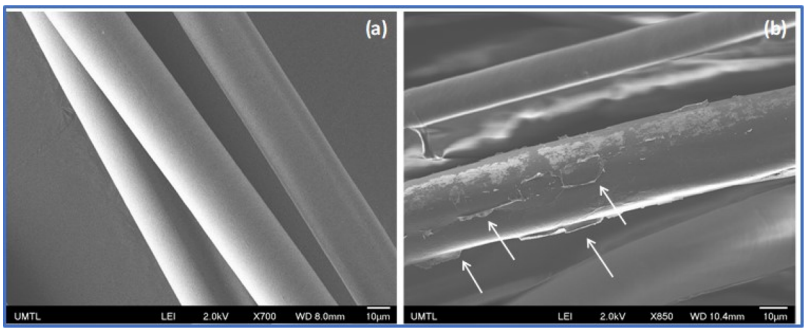

Figure 7. SEM images of (a) dewaxed fibers and (b) GO-treated milkweed fibers. The arrows show the GO layer deposed on the fiber surface.

number of germination sites on the surface of natural fibers because of the high surface energy. The formation of these germs reduces the energy of the system and they are very abundant on the surface of the fibers. Germinations are, therefore, heterogeneous. The high concentration of germinations on the fiber surface conducts to a steric effect during the growth of spherulites, which forces the polymer chains to grow in a single direction, perpendicular to the axis of the fiber where the chains were highly oriented (Figure 5a–f).

The growth rates of the PCL/PVC blends, isothermally crystallized at 35 °C at different PCL contents, were calculated by using the POM technique by measuring the radius change of the spherulite as a function of time. Figure 5a–f shows the development of the crystals on the fiber/polymer interface. The thickness of this layer can be determined by measuring the changes in its radius with crystallization time. The obtained results show that the relationship between the radius of spherulites and crystallization time was linear; thus, the spherulitic growth rate can be extrapolated from these linear curves. The growth rate values are plotted in Figure 5g for various PCL/PVC blends. The addition of PVC leads to a notable decrease in terms of crystallization rate of the blends. However, the spherulitic growth rates at the interface and in the bulk were not necessarily different and they are in the same order of magnitude (Figure 5g).

The formation of the transcrystallization layer may involve the possible interactions between the functional groups of GO and the polymer matrix. The XPS was conducted to identify if there are potential functional groups on the GO surface. Figure 6 shows an HR-TEM image of the prepared GO and a C 1s narrow-XPS spectrum (Figure 6b). Figure 6a shows that the GO was composed of mixed structures represented by the presence of both multilayer stacks (blue arrows) and exfoliated layers of graphite (red arrows) randomly distributed in the carbonaceous matrix. The average interlayer distance between these graphene layers was measured to be 3.5 Å which becomes larger in the exfoliated regions. The high-resolution spectrum of the C 1s region (Figure 6b) gives an asymmetric and complex peak, which was fitted with five main components centered at 284.2, 285.6, 286.7, 288.5, and 290.5 eV, corresponding to sp^2 carbon (C═C), sp^3 carbon (C−C/C−H), C−O, C═O, and $\pi-\pi^*$ shake-up satellites, respectively. The high relative area of the sp^2 carbon peak (compared to that of sp^3) and the presence of the shake-up, which is characteristic of the aromatic compounds, clearly indicate the formation of graphene sheets. However, the presence of epoxy or alcohol groups (C−O−C and C−OH), carboxylic acid functions (HO−C═O), and sp^3 hybridized carbon (C−C, C−H) suggests the surface oxidation of a fraction of the graphene. This helps to prove the existence of functional groups in the GO surface that promote the transcrystallization layer.

The SEM images of the fibers before and after treatment with graphene were also recorded to evaluate the distribution of graphene on the fiber surface. Figure 7 shows that nontreated fibers (dewaxed only) exhibit a smooth surface while the GO-treated fibers exhibit the presence of a graphene layer (white arrows) on the fiber surface. The presence of GO on the surface of a fiber enhances the surface roughness and/or alters the surface composition, both contributing to enhancing the affinity of a polymer segment to absorb on the GO surface and enhance nucleation through soft-epitaxy, as previously observed.[32]

In some previous publications,[26,27] it was reported that there was a concentration gradient during the crystallization in the PCL/PVC blend. The PCL is found to be more concentrated on the air/polymer interface while the PVC is segregated in the bulk. In other words, the chemical composition of the blend is heterogeneous in the whole blend during crystallization. We

https://dx.doi.org/10.1021/acsomega.0c02913
ACS Omega 2020, 5, 22430−22439

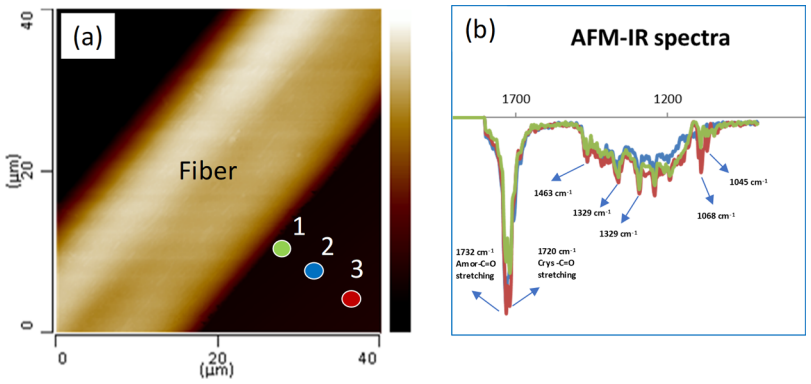

Figure 8. (a) AFM image of the PCV/PVC (80/20) blend showing the analyzed positions and (b) AFM-IR spectra of the PCL/PVC (80/20) near the interface. The distance between the analyzed points (1,2 and 3) is about 5 μm. The colored marker locations on the AFM image correspond to the spectrum of the same color.

believe that the gradient of the concentration is governed by surface tension and the diffusion phenomena in these blends. It is reported that the lower surface energy components in blend systems normally enrich the surface of the blend. It is especially true in the case of PCL/PVC blends in which PCL has a surface tension at room temperature of about 33 dyn/cm[58] while the PVC have solid surface tensions 42.023 dyn/cm,[59] respectively. This phenomenon is also correlated with observations made by Clark et al.[60,61] who have been reported a PCL surface enrichment at the air-polymer interface in PCL/PVC blends because of the development of faster growing spherulites at the surface than in the core, given that the surface of the film is enriched in PCL, and therefore, the dilution effect of the PVC component is less than it is in the core.

In this work, the presence of a polar coated fiber (milkweed) may cause a change in the chemical composition of the blends at the interface because of the difference in the polarity of PCL and PVC. To verify this hypothesis, AFM-IR measurements were made to evaluate the chemical composition in the matrix, especially near the vicinity of fiber/polymer interface. Figure 8 shows AFM-IR spectra pointed on the IR fingerprint region (900−1800 cm^{-1}). Various characteristic peaks linked to the PCL/PVC blend were observed. The bands at 1715 and 1732 cm^{-1} were attributed to the axial deformation of the carbonyl group in the crystalline and amorphous states, respectively. This is because the AFM-IR is more resolved than the traditional FT-IR and thus the crystallinity of the polymer can be calculated at the nanoscale.[10,11,19] The bands at 1395 and 1329 cm^{-1} were assigned to the symmetric angular deformation of CH and axial deformation of C−O, respectively. The band at 1463 cm^{-1} was attributed to the angular deformation of C−H while the bands at 1068 and 1045 cm^{-1} were attributed to the axial deformation of O−C−C.[62] However, because of the limit of the AFM-IR laser resource, the band at 746 cm^{-1}, assigned to the axial deformation of C−Cl is lacking.

The relationship between the intensity of the crystalline (I_{1715}) and amorphous (I_{1732}) bands, assigned to carbonyl groups, was also calculated. The values are found to be 0.97, 1.01, and 1.09 for the locations 1, 2, and 3 on the AFM image, respectively (Figure 8a). It is interesting to see that the I_{1715}/I_{1732} ratios decrease when the AFM tip moves away from the interface, meaning that there is an increase of the crystallinity degree from the transcrystallization layer to the matrix. This may involve the rejection of PCL amorphous during crystallization. More specifically, a fraction of the PCL component can be rejected from the vicinity of the interface into the bulk under confinement conditions and be subjected to local interactions leading to PCL chains in different conformations. This suggestion is supported by a recent publication by Liang et al. by using scanning nanoscale microbeam dimensional wide-angle X-ray diffraction (2D-WAXD) measurement for which they have found that the crystallinity of PLA is notably higher in the transcrystallization layer compared to that observed in the matrix.[31]

3. CONCLUSIONS

We demonstrated that the transcrystallization of the PCL/PVC on the milkweed fiber is significantly enhanced by simply coating the fiber with a layer of graphene oxide. The presence of the GO layer on the fiber surface promotes the nucleation sites and improves the chemical interactions between the fiber surface and the polymer blends. By using AFM-IR, we demonstrated, for the first time, that there is a segregation of polymers during the crystallization at the vicinity of the interface for which the crystallinity of PCL/PVC is higher in the transcrystallization layer compared to that in the bulk.

The kinetics of the interfacial crystallization, as well as the nanoscale characterization of the synthesized GO are also reported. The addition of PVC slows down the crystal growth rate of the PCL. The results of this work provide useful information to similar studies on the interfacial crystallization of natural fiber and miscible PCL/PVC blends. Future works will be focused to provide a better understanding of the lamellar assembly in the transcrystallization layer and to quantitatively determine the segregation phenomena of the blends during the isothermal crystallization.

4. MATERIALS AND METHODS

4.1. Materials. Common milkweed fibers (*Asclepias syriaca*) were harvested from a local farm in Granby (Quebec, Canada). Upon measurement, the average cell wall thickness and fiber diameter were found to be 900 ± 120 and 20 ± 3 μm, respectively (Figure 1). They were treated with chloroform for 10 min to remove any waxes from their surfaces. In some cases, these fibers were pretreated with graphene oxide solutions for 5 min at different concentrations (0, 0.15 and 0.35 mg/mL) to promote the development of the transcrystallization layer. PCL, with an average molecular weight

https://dx.doi.org/10.1021/acsomega.0c02913
ACS Omega 2020, 5, 22430−22439

(M_w) of 10,000 g/mol, melting point (T_m) of 60 °C, and glass transition temperature (T_g) of −59 °C (measured by differential scanning calorimetry, DSC), was supplied by Sigma-Aldrich Canada. Polyvinyl chloride (PVC), with an average M_w of 67,000 g/mol and T_g of 80 °C (measured by DSC); was supplied by Sigma-Aldrich Canada. Tetrahydrofuran (THF) and chloroform ($CHCl_3$) used in this study were of analytical grade.

4.2. Synthesis of Graphene Oxide. Graphene oxide was synthesized by the modified Hummer method from graphite.[40] A resulting dark powder was obtained, which underwent an ultrasonication process in water and was dried to remove moisture. The HR-TEM shows a basal distance of about 0.3 nm. These materials contain various oxygen-containing functional groups as described by using XPS (Figure 6, Section 4.4).

The single composite was prepared as follows: a single fiber was first deposited and fixed on an optical glass sheet. In the next step, a solution of polymers (PCL or its blends), dissolved in tetrahydrofuran (THF) at different concentrations, was dropped on the fiber surface. The sample was dried at room temperature in a vacuum oven for 24 h before analyzing by POM (Section 4.3.3).

4.3. Characterization Methods. *4.3.1. Atomic Force Microscope Infrared Spectroscopy.* The AFM-IR measurements were carried out using a Nano-IR2 system (Anasys Instruments, CA, USA). The AFM images were recorded in the contact mode with a rate line of 0.1−1 Hz using a gold-plated silicon nitride probe (Anasys Instruments, CA, USA) with an elastic constant of about 0.5 $N.m^{-1}$ and a nominal radius of 10 nm. The nanoscale IR spectra were collected directly on a single fiber surface or polymeric film, within the 900−1800 cm^{-1} range at a spectral resolution of 4 cm^{-1}, 256 co-averages, with at least 10 measurements. The single IR radiation image was recorded with a scan rate of 0.1 Hz, resolution of 512 × 512 pixels, and 16 co-averages at a power limit within 0.3−10% at a frequency of 86 Hz. All the measurements were carried out at room temperature in a humidity-controlled room as described in our previous publications.[10,11,37−39]

4.3.2. High-Resolution Transmission Electron Microscopy. HR-TEM was performed using a JEOL 2170F (JEOL Inc., Tokyo, JAPAN) at a 200 kV acceleration voltage. EDS spectra were acquired with an Oxford EDS detector and INCA software. Images were acquired with Gatan's Digital Micrograph software using a 4-megapixel CCD camera. The basal distance is calculated by using Image J software and the reported values are averaged.

4.3.3. Polarized Optical Microscopy. A Zeiss Axioskop polarizing microscope equipped with a Linkman temperature controller and cooling system with liquid nitrogen was used in this study. The optical micrographs were recorded by a digital camera (HV-D273CCD). For isothermal crystallization investigation, samples were heated to 100 °C at a heating rate of 10 °C/min and kept at this temperature for 3 min to a full melting of all crystals. The system was then quickly cooled to the desired temperature (35, 40 and 45 °C) to observe the spherulite growth as a function of time. Image-Pro Plus software was used to calculate the spherulite dimensions.

4.3.4. X-Ray Photoelectron Spectroscopy. XPS of the prepared GO were performed using a Thermo Scientific K-Alpha spectrometer equipped with a monochromatic Al Kα X-ray source ($h\nu$ = 1486 eV). The spot size was 400 μm, while the pass energy of surveys and the high-energy resolution was set to 200 and 50 eV, respectively. Deconvolution was performed using Thermo-Advantage software.

4.3.5. Gas Chromatography−Mass Spectrometry (GC−MS). The chemical composition of waxes, extracted from the fiber surface by using chloroform was analyzed by gas chromatography−mass spectrometry (GC−MS) (Agilent Technologies, 7890A GC/MS) equipped with an HP-5MS column (Agilent Technologies Inc., Santa Clara, CA, USA). The temperature was regulated from 160 to 300 °C at 5 °C/min. The carrier gas was helium at a flow rate of 1 mL/min with a split ratio of 15:1. The injection and detection temperatures were both set at 300 °C with an electronic ionization voltage of 70 eV and an EM voltage of 1871 mV.

AUTHOR INFORMATION

Corresponding Author

Phuong Nguyen-Tri − *Department of Chemistry, Biochemistry and Physics, University du Québec à Trois-Rivières, Trois-Rivieres G9A 5H7, Québec, Canada;* orcid.org/0000-0001-6578-5716; Phone: + 819-376 5011 (4505); Email: Phuong.nguyen-tri@uqtr.ca

Authors

Pascal Carrière − *Laboratoire des Matériaux, Polymères, Interfaces et Environnement Marin (MAPIEM), Université de Toulon, La Garde 83130, France*

Adam Duong − *Department of Chemistry, Biochemistry and Physics, University du Québec à Trois-Rivières, Trois-Rivieres G9A 5H7, Québec, Canada;* orcid.org/0000-0002-4927-3603

Sonil Nanda − *Department of Chemical and Biological Engineering, University of Saskatchewan, Saskatoon S7N 5A9, Saskatchewan, Canada*

Complete contact information is available at: https://pubs.acs.org/10.1021/acsomega.0c02913

Notes

The authors declare no competing financial interest.

ACKNOWLEDGMENTS

Natural Sciences and Engineering Research Council of Canada (NSERC) is thanked for the financial support. We thank P. Moraille (University of Montreal, Canada) for her kind help in AFM-IR measurements and Dr A. Fahs (University of Toulon, France) for his SEM fiber characterization. Thanks to Prof. Robert E. Prud'homme (University of Montreal) for his useful comments during the realization of this work.

REFERENCES

(1) Lotz, B.; Miyoshi, T.; Cheng, S. Z. D. 50th Anniversary Perspective: Polymer Crystals and Crystallization: Personal Journeys in a Challenging Research Field. *Macromolecules* **2017**, *50*, 5995−6025.

(2) Zhang, M.; Guo, B.-H.; Xu, J. A Review on Polymer Crystallization Theories. *Crystals* **2016**, *7*, 4.

(3) Gao, X.-R.; Li, Y.; Huang, H.-D.; Xu, J.-Z.; Xu, L.; Ji, X.; Zhong, G.-J.; Li, Z.-M. Extensional Stress-Induced Orientation and Crystallization can Regulate the Balance of Toughness and Stiffness of Polylactide Films: Interplay of Oriented Amorphous Chains and Crystallites. *Macromolecules* **2019**, *52*, 5278−5288.

(4) Sarasua, J.-R.; Rodríguez, N. L.; Arraiza, A. L.; Meaurio, E. Stereoselective Crystallization and Specific Interactions in Polylactides. *Macromolecules* **2005**, *38*, 8362−8371.

(5) Feng, C.; Chen, Y.; Shao, J.; Hou, H. The Crystallization Behavior of Poly(l-lactic acid)/Poly(d-lactic acid) Electrospun Fibers: Effect of Distance of Isomeric Polymers. *Ind. Eng. Chem. Res.* **2020**, *59*, 8480−8491.
(6) Liu, C.; Noda, I.; Chase, D. B.; Zhang, Y.; Qu, J.; Jia, M.; Ni, C.; Rabolt, J. F. Crystallization Retardation of Ultrathin Films of Poly[(R)-3-hydroxybutyrate] and a Random Copolymer Poly[(R)-3-hydroxybutyrate-co-(R)-3-hydroxyhexanoate] on an Aluminum Oxide Surface. *Macromolecules* **2019**, *52*, 7343−7352.
(7) Wang, D.; Russell, T. P. Advances in Atomic Force Microscopy for Probing Polymer Structure and Properties. *Macromolecules* **2018**, *51*, 3−24.
(8) Tahara, D.; Ninh, T. H.; Yamamoto, H.; Tashiro, K. Metropolis Monte Carlo Simulation of Two-Dimensional Small-Angle X-ray Scattering Patterns of Oriented Polymer Materials. *Macromolecules* **2020**, *53*, 276−287.
(9) Prud'homme, R. E. Crystallization and morphology of ultrathin films of homopolymers and polymer blends. *Prog. Polym. Sci.* **2016**, *54*−*55*, 214−231.
(10) Nguyen Tri, P.; Prud'homme, R. E. Crystallization and Segregation Behavior at the Submicrometer Scale of PCL/PEG Blends. *Macromolecules* **2018**, *51*, 7266−7273.
(11) Tri, P. N.; Prud'homme, R. E. Nanoscale Lamellar Assembly and Segregation Mechanism of Poly(3-hydroxybutyrate)/Poly-(ethylene glycol) Blends. *Macromolecules* **2018**, *51*, 181−188.
(12) Dazzi, A.; Prater, C. B. AFM-IR: Technology and Applications in Nanoscale Infrared Spectroscopy and Chemical Imaging. *Chem. Rev.* **2017**, *117*, 5146−5173.
(13) Ghosh, S.; Kouamé, N. A.; Ramos, L.; Remita, S.; Dazzi, A.; Deniset-Besseau, A.; Beaunier, P.; Goubard, F.; Aubert, P.-H.; Remita, H. Conducting polymer nanostructures for photocatalysis under visible light. *Nat. Mater.* **2015**, *14*, 505−511.
(14) Cavezza, F.; Pletincx, S.; Revilla, R. I.; Weaytens, J.; Boehm, M.; Terryn, H.; Hauffman, T. Probing the Metal Oxide/Polymer Molecular Hybrid Interfaces with Nanoscale Resolution Using AFM-IR. *J. Phys. Chem. C* **2019**, *123*, 26178−26184.
(15) Rao, V. J.; Matthiesen, M.; Goetz, K. P.; Huck, C.; Yim, C.; Siris, R.; Han, J.; Hahn, S.; Bunz, U. H. F.; Dreuw, A.; Duesberg, G. S.; Pucci, A.; Zaumseil, J. AFM-IR and IR-SNOM for the Characterization of Small Molecule Organic Semiconductors. *J. Phys. Chem. C* **2020**, *124*, 5331−5344.
(16) Waeytens, J.; Doneux, T.; Napolitano, S. Evaluating Mechanical Properties of Polymers at the Nanoscale Level via Atomic Force Microscopy−Infrared Spectroscopy. *ACS Appl. Polym. Mater.* **2019**, *1*, 3−7.
(17) Rao, V. J.; Matthiesen, M.; Goetz, K. P.; Huck, C.; Yim, C.; Siris, R.; Han, J.; Hahn, S.; Bunz, U. H. F.; Dreuw, A.; Duesberg, G. S.; Pucci, A.; Zaumseil, J. AFM-IR and IR-SNOM for the Characterization of Small Molecule Organic Semiconductors. *J. Phys. Chem. C* **2020**, *124*, 5331−5344.
(18) Huang, L.; Zhang, X.; Shao, J.; Zhou, Z.; Chen, Y.; Hu, X. Nanoscale chemical and mechanical heterogeneity of human dentin characterized by AFM-IR and bimodal AFM. *J. Adv. Res.* **2020**, *22*, 163−171.
(19) Gong, L.; Chase, D. B.; Noda, I.; Liu, J.; Martin, D. C.; Ni, C.; Rabolt, J. F. Discovery of β-Form Crystal Structure in Electrospun Poly[(R)-3-hydroxybutyrate-co-(R)-3-hydroxyhexanoate] (PHBHx) Nanofibers: From Fiber Mats to Single Fibers. *Macromolecules* **2015**, *48*, 6197−6205.
(20) Rahmani Del Bakhshayesh, A.; Mostafavi, E.; Alizadeh, E.; Asadi, N.; Akbarzadeh, A.; Davaran, S. Fabrication of Three-Dimensional Scaffolds Based on Nano-biomimetic Collagen Hybrid Constructs for Skin Tissue Engineering. *ACS Omega* **2018**, *3*, 8605−8611.
(21) Torres, E.; Fombuena, V.; Vallés-Lluch, A.; Ellingham, T. Improvement of mechanical and biological properties of Polycaprolactone loaded with Hydroxyapatite and Halloysite nanotubes. *Mater. Sci. Eng., C* **2017**, *75*, 418−424.
(22) Chang, S. H.; Lee, H. J.; Park, S.; Kim, Y.; Jeong, B. Fast Degradable Polycaprolactone for Drug Delivery. *Biomacromolecules* **2018**, *19*, 2302−2307.
(23) Gao, X.; Song, J.; Zhang, Y.; Xu, X.; Zhang, S.; Ji, P.; Wei, S. Bioinspired Design of Polycaprolactone Composite Nanofibers as Artificial Bone Extracellular Matrix for Bone Regeneration Application. *ACS Appl. Mater. Interfaces* **2016**, *8*, 27594−27610.
(24) Nyitray, C. E.; Chang, R.; Faleo, G.; Lance, K. D.; Bernards, D. A.; Tang, Q.; Desai, T. A. Polycaprolactone Thin-Film Micro- and Nanoporous Cell-Encapsulation Devices. *ACS Nano* **2015**, *9*, 5675−5682.
(25) Latini, G.; Ferri, M.; Chiellini, F. Materials Degradation in PVC Medical Devices, DEHP Leaching and Neonatal Outcomes. *Curr. Med. Chem.* **2010**, *17*, 2979−2989.
(26) Mareau, V. H.; Prud'homme, R. E. Growth Rates and Morphologies of Miscible PCL/PVC Blend Thin and Thick Films. *Macromolecules* **2003**, *36*, 675−684.
(27) Mamun, A.; Bazuin, C. G.; Prud'homme, R. E. Morphologies of Various Polycaprolactone/Polymer Blends in Ultrathin Films. *Macromolecules* **2015**, *48*, 1412−1417.
(28) Mamun, A.; Mareau, V. H.; Chen, J.; Prud'homme, R. E. Morphologies of miscible PCL/PVC blends confined in ultrathin films. *Polymer* **2014**, *55*, 2179−2187.
(29) Martins-Franchetti, S. M.; Campos, A.; Egerton, T. A.; White, J. R. Structural and morphological changes in Poly(caprolactone)/poly(vinyl chloride) blends caused by UV irradiation. *J. Mater. Sci.* **2007**, *43*, 1063−1069.
(30) Xu, H.; Xie, L.; Jiang, X.; Li, X.-J.; Li, Y.; Zhang, Z.-J.; Zhong, G.-J.; Li, Z.-M. Toward Stronger Transcrystalline Layers in Poly(l-lactic acid)/Natural Fiber Biocomposites with the Aid of an Accelerator of Chain Mobility. *J. Phys. Chem. B* **2014**, *118*, 812−823.
(31) Liang, Y.-Y.; Xu, J.-Z.; Li, Y.; Zhong, G.-J.; Wang, R.; Li, Z.-M. Promoting Interfacial Transcrystallization in Polylactide/Ramie Fiber Composites by Utilizing Stereocomplex Crystals. *ACS Sustainable Chem. Eng.* **2017**, *5*, 7128−7136.
(32) Abdou, J. P.; Braggin, G. A.; Luo, Y.; Stevenson, A. R.; Chun, D.; Zhang, S. Graphene-Induced Oriented Interfacial Microstructures in Single Fiber Polymer Composites. *ACS Appl. Mater. Interfaces* **2015**, *7*, 13620−13626.
(33) Kim, T.; Jeon, H.; Jegal, J.; Kim, J. H.; Yang, H.; Park, J.; Oh, D. X.; Hwang, S. Y. Trans crystallization behavior and strong reinforcement effect of cellulose nanocrystals on reinforced poly-(butylene succinate) nanocomposites. *RSC Adv.* **2018**, *8*, 15389−15398.
(34) Dufresne, A.; Kellerhals, M. B.; Witholt, B. Transcrystallization in Mcl-PHAs/Cellulose Whiskers Composites. *Macromolecules* **1999**, *32*, 7396−7401.
(35) Hassanzadeh, S.; Hasani, H. A Review on Milkweed Fiber Properties as a High-Potential Raw Material in Textile Applications. *J. Ind. Text.* **2016**, *46*, 1412−1436.
(36) Richard, C.; Cousin, P.; Foruzanmehr, M.; Elkoun, S.; Robert, M. Characterization of components of milkweed floss fiber. *Sep. Sci. Technol.* **2018**, *54*, 3091−3099.
(37) Nguyen, T. V.; Le, X. H.; Dao, P. H.; Decker, C.; Nguyen-Tri, P. Stability of acrylic polyurethane coatings under accelerated aging tests and natural outdoor exposure: The critical role of the used photo-stabilizers. *Prog. Org. Coat.* **2018**, *124*, 137−146.
(38) Nguyen-Tri, P.; Prud'homme, R. E. Nanoscale analysis of the photodegradation of Polyester fibers by AFM-IR. *J. Photochem. Photobiol., A* **2019**, *371*, 196−204.
(39) Zeb, G.; Tri, P. N.; Palacin, S.; Le, X. T. Pulse potential deposition of thick polyvinylpyridine-like film on the surface of titanium nitride. *RSC Adv.* **2016**, *6*, 80825−80829.
(40) Marcano, D. C.; Kosynkin, D. V.; Berlin, J. M.; Sinitskii, A.; Sun, Z.; Slesarev, A.; Alemany, L. B.; Lu, W.; Tour, J. M. Improved Synthesis of Graphene Oxide. *ACS Nano* **2010**, *4*, 4806−4814.
(41) Ensikat, H. J.; Ditsche-Kuru, P.; Neinhuis, C.; Barthlott, W. Superhydrophobicity in perfection: the outstanding properties of the lotus leaf. *Beilstein J. Nanotechnol.* **2011**, *2*, 152−161.

https://dx.doi.org/10.1021/acsomega.0c02913
ACS Omega 2020, 5, 22430−22439

(42) Koch, K.; Dommisse, A.; Barthlott, W. Chemistry and Crystal Growth of Plant Wax Tubules of Lotus (Nelumbo nucifera) and Nasturtium (Tropaeolum majus) Leaves on Technical Substrates. *Cryst. Growth Des.* **2006**, *6*, 2571−2578.
(43) Hojilla-Evangelista, M. P.; Evangelista, R. L.; Victor Wu, Y. Characterization of milkweed (Asclepias spp.) seed proteins. *Ind. Crops Prod.* **2009**, *29*, 275−280.
(44) Richard, C.; Cousin, P.; Foruzanmehr, M.; Elkoun, S.; Robert, M. Characterization of components of milkweed floss fiber. *Sep. Sci. Technol.* **2019**, *54*, 3091−3099.
(45) Woo, E. M.; Wu, P. L.; Wu, M. C.; Yan, K. C. Thermal Behavior of Ring-Band versus Maltese-Cross Spherulites: Case of Monomorphic Poly(ethylene adipate). *Macromol. Chem. Phys.* **2006**, *207*, 2232−2243.
(46) Wang, Z.; Alfonso, G. C.; Hu, Z.; Zhang, J.; He, T. Rhythmic Growth-Induced Ring-Banded Spherulites with Radial Periodic Variation of Thicknesses Grown from Poly(ε-caprolactone) Solution with Constant Concentration. *Macromolecules* **2008**, *41*, 7584−7595.
(47) Zhang, Q.; Fan, J.; Feng, J. Formation of banded spherulites and the temperature dependence of the band space in olefin block copolymer. *RSC Adv.* **2015**, *5*, 43155−43163.
(48) Li, Y.; Huang, H.; Wang, Z.; He, T. Tuning Radial Lamellar Packing and Orientation into Diverse Ring-Banded Spherulites: Effects of Structural Feature and Crystallization Condition. *Macromolecules* **2014**, *47*, 1783−1792.
(49) Takahashi, S.; Kiran, E. Development of ring-banded spherulitic morphologies and formation of radially oriented nano-pores in poly(3-hydroxybutyrate-co-3-hydroxyvalerate) during crystallization in CO_2. *J. Supercrit. Fluids* **2015**, *96*, 359−368.
(50) Ding, G.; Liu, J. Morphological varieties and kinetic behaviors of poly(3-hydroxybutyrate) (PHB) spherulites crystallized isothermally from thin melt film. *Colloid Polym. Sci.* **2013**, *291*, 1547−1554.
(51) Wang, Z.; Alfonso, G. C.; Hu, Z.; Zhang, J.; He, T. Rhythmic Growth-Induced Ring-Banded Spherulites with Radial Periodic Variation of Thicknesses Grown from Poly(ε-caprolactone) Solution with Constant Concentration. *Macromolecules* **2008**, *41*, 7584−7595.
(52) Ishida, H.; Bussi, P. Surface induced crystallization in ultrahigh-modulus polyethylene fiber-reinforced polyethylene composites. *Macromolecules* **1991**, *24*, 3569−3577.
(53) Cho, K.; Kim, D.; Yoon, S. Effect of Substrate Surface Energy on Transcrystalline Growth and Its Effect on Interfacial Adhesion of Semicrystalline Polymers. *Macromolecules* **2003**, *36*, 7652−7660.
(54) Li, Z.-M.; Li, L.-B.; Shen, K.-Z.; Yang, W.; Huang, R.; Yang, M.-B. Transcrystalline Morphology of an in situ Microfibrillar Poly(ethylene terephthalate)/Poly(propylene) Blend Fabricated through a Slit Extrusion Hot Stretching-Quenching Process. *Macromol. Rapid Commun.* **2004**, *25*, 553−558.
(55) Sun, R.; Feng, Y.; Wang, B.; Liu, C.; Shen, C. Enhanced interfacial and mechanical property of biodegradable poly(butylene succinate) film via introducing ultrahigh molecular weight polyethylene shish-kebab fibers. *Mater. Res. Express* **2020**, *6*, 125374.
(56) Jenckel, E.; Teege, E.; Hinrichs, W. Transkristallisation in hochmolekularen Stoffen. *Kolloid-Z.* **1952**, *129*, 19−24.
(57) Quan, H.; Li, Z.-M.; Yang, M.-B.; Huang, R. On transcrystallinity in semi-crystalline polymer composites. *Compos. Sci. Technol.* **2005**, *65*, 999−1021.
(58) He, Y.; Wildman, R. D.; Tuck, C. J.; Christie, S. D. R.; Edmondson, S. An Investigation of the Behavior of Solvent based Polycaprolactone ink for Material Jetting. *Sci. Rep.* **2016**, *6*, 20852.
(59) Schmidt, J. J.; Gardella, J. A.; Salvati, L. Surface studies of polymer blends. 2. An ESCA and IR study of poly(methyl methacrylate)/poly(vinyl chloride) homopolymer blends. *Macromolecules* **1989**, *22*, 4489−4495.
(60) Clark, M. B.; Burkhardt, C. A.; Gardella, J. A. Surface studies of polymer blends. 3. An ESCA, IR and DSC study of poly(epsilon.-caprolactone)/poly(vinyl chloride) homopolymer blends. *Macromolecules* **1989**, *22*, 4495−4501.
(61) Mareau, V. H.; Prud'homme, R. E. Dual Growth Rates and Morphologies of Isothermally Crystallized Miscible Polymer Blends. *Macromolecules* **2002**, *35*, 5338−5341.
(62) Campos, A. d.; Marconato, J. C.; Martins-Franchetti, S. M. The influence of soil and landfill leachate microorganisms in the degradation of PVC/PCL films cast from DMF. *Polimeros* **2012**, *22*, 220−227.

https://dx.doi.org/10.1021/acsomega.0c02913
ACS Omega 2020, 5, 22430−22439